

**CHARACTERISATION AND RADIATION
SHIELDING PROPERTIES OF COMMERCIAL
CERAMIC MATERIALS USING KILOVOLTAGE
PHOTON BEAM**

MOHD AIZUDDIN BIN ZAKARIA

UNIVERSITI SAINS MALAYSIA

2024

**CHARACTERISATION AND RADIATION
SHIELDING PROPERTIES OF COMMERCIAL
CERAMIC MATERIALS USING KILOVOLTAGE
PHOTON BEAM**

by

MOHD AIZUDDIN BIN ZAKARIA

Thesis submitted in fulfilment of the requirements

for the degree of

Master of Science

November 2024

ACKNOWLEDGEMENT

In the name of Allah, the Most Gracious and Most Merciful. Alhamdulillah, all praises to almighty Allah s.w.t for all the strength to complete my master's degree. I would like to express my sincerest gratitude to all those who were directly and indirectly involved in fulfilling this masters research study. My utmost appreciation goes to all those who made it possible to complete this study, especially my supervisor Associate Professor Dr. Mohd Zahri bin Abdul Aziz from Advanced Dental and Medical Institute, USM, and my two co-supervisors Dr. Mohammad Khairul Azhar Abdul Razab and Mr. Mohd Zulfadli Adenan. This study would not have been possible without the support and guidance from my supervisor and co supervisors. I am deeply grateful to them. I would also like to extend my gratitude to the programme director and all the staff members of Medical Imaging Programme, UiTM, Puncak Alam, for giving me permission to operate the X-ray machine. This has given such significance to the quality of my research. Not to forget the staff members of ADMI, which allows access to research tools such as MC PHITS and virtual library. Finally, my warm thanks and appreciation to my parents and spouse who have provided moral support and encouragement throughout this journey as a student. Their patience and understanding have been a constant source of strength. I am also grateful to the support group amongst my colleagues and friends, which generously gave motivation and advice to this study. Overall, this journey as a master student in medical physics has been an amazing learning experience that is unique and different from my previous undergraduate studies.

TABLE OF CONTENTS

ACKNOWLEDGEMENT	ii
TABLE OF CONTENTS	iii
LIST OF TABLES	vii
LIST OF FIGURES	ix
LIST OF SYMBOLS AND ABBREVIATIONS	xiv
ABSTRAK	xix
ABSTRACT	xxi
CHAPTER 1 INTRODUCTION	1
1.1 Background	1
1.2 Problem statement	6
1.3 Objective of research.....	8
1.4 Significance of study	8
1.5 Outline of thesis	9
1.6 Scope of Study	10
CHAPTER 2 THEORY & LITERATURE REVIEW	12
2.1 X-ray Interactions.....	12
2.2 Radiation Shielding Properties.....	17
2.3 Radiation Concept and Units.....	21
2.4 Radiology Diagnostic Room Design and Shielding.....	23
2.5 Classification of ceramic tiles	30
2.6 The Compound Properties Ceramic	31
2.7 Manufacturing of The Ceramic	34
2.8 Ceramic Materials as Radiation Shielding Against Diagnostic Photon Energy	39

2.9	MC Modelling, Simulation and Validation	43
CHAPTER 3 MATERIAL AND METHODS.....		51
3.1	Characterisation of Ceramic Material	51
3.2	Selection of Ceramic as Sample.....	54
3.2.1	Measurement of Ceramic Tile Density	58
3.2.2	Radiation Shielding Properties.....	59
3.2.2(a)	Preparation of the ceramic samples for FESEM, and EDX analysis	60
3.2.2(b)	Characterisation Analysis of Surface and Cross Section Using Field Emission Scanning electron microscopy (FESEM)	61
3.2.2(c)	Analysis of Ceramic Elements Using Energy Dispersive X-ray (EDX) Spectroscopy	67
3.2.2(d)	Sample Preparation for the Analysis of Ceramic Compound using X-ray Fluoroscopy (XRF)	68
3.3	Evaluation of Shielding Characteristics Data for KV Photon Beam	72
3.4	Establishment of a Validated MC Beam Model.....	77
3.4.1	PHITS Simulation System Model.....	78
3.4.2	Monte Carlo Simulation Parameter.....	79
3.4.3	Input Simulation Code for Parameter.....	80
3.4.4	Input data for [Source] section.....	82
3.4.5	Experimental simulation setup.....	85
3.4.6	Simulation to measure lead Equivalent and shielding power (absorbed percentage)	86
3.4.7	Development of X-ray room layout geometry for PHITS modelling.....	88
3.4.8	Input data for Room Material, Surface Dimension and Cell Information.....	93
3.4.9	Input Data for [T-Track]	97
3.4.10	Radiation unit and conversion.....	97

CHAPTER 4	RESULTS AND DISCUSSIONS	100
4.1	Characterisation of the Ceramic.....	102
4.1.1	Morphological Properties and Characteristics of Ceramic	102
4.1.2	Measurement of Pore Sizes and Area Fraction Pores from FESEM Cross Section Micrograph Image	123
4.1.3	Element Composition properties	128
4.1.4	XRF Compound Properties	133
4.2	Evaluation of Shielding Characteristics Data for KV Photon Beam.....	135
4.2.1	Average Exposure for Ceramic	136
4.2.2	Linear Attenuation Coefficient (LAC).....	137
4.2.3	Half-Value Layer (HVL).....	140
4.2.4	Mass Attenuation Coefficient (MAC).....	142
4.2.5	Mean Free Path (MFP).....	145
4.2.6	Total Molecular Cross-Section (σ_t) , Total Atomic Cross- Section (σ_a), and Total Electronic Cross-Section (σ_e).....	147
4.3	Establishment of a Validated MC Beam Model	149
4.3.1	Validation of the experimental setup	150
4.3.2	Evaluation of Ceramic Shielding Capabilities by Measuring Ceramic Attenuation Using Verified Simulation Setup.....	154
4.3.3	The Lead Equivalent Thickness of the Selected Ceramic Samples	165
4.3.4	Fluence Distribution Across the Room	167
4.3.5	Simulation X-ray room model.....	170
CHAPTER 5	CONCLUSION AND FUTURE RECOMMENDATIONS....	178
5.1	Conclusion.....	178
5.2	Recommendations	182
REFERENCES.....		184
APPENDICES		

LIST OF PUBLICATION

LIST OF TABLES

	Page
Table 2.1 Summary of the Study of Different type of Material as Shielding Material	49
Table 3.1 Selected Brands and Types of ceramic tiles.	55
Table 3.2 Measurement of the room.....	93
Table 3.3 Input instruction for [material]	93
Table 3.4 Input instruction for [Cell].....	94
Table 3.5 Input instruction for [Surface]	95
Table 4.1 Classification of ceramic.	101
Table 4.2 Area pore size from FESEM Image.	126
Table 4.3 EDX single element for cross section of the ceramic tile for samples C1 to C12.	129
Table 4.4 EDX single element for surface of the ceramic tile for samples C1 to C12.	130
Table 4.5 Ratio Nonmetal and Metalloid to metal elements.	132
Table 4.6 Chemical Composition of Selected Ceramic Tiles obtained using XRF.	133
Table 4.7 Measurement of Average Exposure (mR).	137
Table 4.8 Linear attenuation coefficient (LAC) for sample C1-C12.....	139
Table 4.9 HVL (cm) for 40, 50, 60, 80, 100, 120, 140 and 150 kVp with constant 10 mAs.....	141
Table 4.10 Mass Attenuation Coefficient (MAC) for Ceramic Tile Sample.	144
Table 4.11 Value of Mean Free Path for Ceramic Tile Sample C1-S1 to C12-S11.	146

Table 4.12	Total atomic Cross Section, Total Electronic Criss-Section, and Effective Atomic Number.	148
Table 4.13	The Discrepancy of Linear Attenuation Coefficient between Experimental and Simulation at energy 40 kV, 80 kV and 150 kV for sample C3-S3, C5-S9 and C8-S4.	153
Table 4.14	Thickness Required to Attenuate More Than 99% of Radiation for Ceramic Tile Sample C3-C3, C5-S9 and C8-S4 at 40 kV.....	156
Table 4.15	Thickness Required to Attenuate More Than 99% of Radiation for Ceramic Tile Sample C3-C3, C5-S9 and C8-S4 at 80 kV.....	159
Table 4.16	Thickness Required to Attenuate More Than 99% of Radiation for Ceramic Tile Sample C3-S3, C5-S9 and C8-S4 at Energy 150 kV	162
Table 4.17	Thickness of selected sample in study, necessary to reduce the intensity equal to 2 mm lead.....	166
Table 4.18	Exposure (mR) at location.....	176

LIST OF FIGURES

	Page
Figure 1.1 The workflow towards the evaluation of ceramic tiles.....	6
Figure 2.1 A diagram of the phenomenon of coherent scattering. Model were adapted from The Essential Physics of Medical Imaging (4 th ed.) by Bushberg, Seibert, Leidholdt, and Boone, coherent scattering (Rayleigh scattering) Chapter 3, Page 39.....	14
Figure 2.2 A Model Diagram of Compton scattering adapted from The Essential Physics of Medical Imaging (4 th ed.) by Bushberg, Seibert, Leidholdt, and Boone chapter 3, Page 40.	16
Figure 2.3 Concept of manufacturing process for ceramic tiles.	37
Figure 3.1 Image of ceramic tile sample C1-S1 to C8-S4.	56
Figure 3.2 Image of ceramic tile sample C9-S5 to C12-S11.	57
Figure 3.3 Digital scale to measure weight of prepared ceramic tiles.....	59
Figure 3.4 Operating System for FESEM and EDX machine were controlled using the desktop operating system.....	62
Figure 3.5 FESEM provide a high-resolution micrograph surface images in which the surface of the ceramic samples is scanned with an electron beam. ..	63
Figure 3.6 Energy dispersive X-ray spectroscopy (EDX) use to measure the element of the ceramic sample.	64
Figure 3.7 Preparation of ceramic tile for FESEM, EDX and XRD.....	66
Figure 3.8 Fiji ImageJ software to analyse the pores structure of the FESEM micrograph.....	67
Figure 3.9 Energy Dispersive X-ray Fluorescence (EDXRF) equipment and operating system.	70
Figure 3.10 Heavy Duty, Planetary Ball Mill, Pulverisette 6 are used to ground down the samples into 250 μm homogenous size.	71

Figure 3.11	10 mg of homogeneous samples inserted into the plastic container before inserting to the XRF instruments.....	72
Figure 3.12	Radcal Rapid-Gold+, AGMS-D+ Detector.	75
Figure 3.13	The Experimental Setup to Evaluate the Ceramic Shielding.	77
Figure 3.14	list of subsections (adapted in PHITS manual).	80
Figure 3.15	X-ray photon spectrum of 150 kV as input source for the calculation. The average energy is 56.7 keV (using filter 0.8 mm filter) (This data was generated from - X-ray spectrum generator for Monte Carlo Calculations).	83
Figure 3.16	X-ray photon spectra of 80 kV as input source in the calculation. The average energy is 38.3 keV (using filter 0.8 mm filter) (This data was generated from - X-ray spectrum generator for Monte Carlo Calculations).	84
Figure 3.17	X-ray photon spectra of 40 kV as input source in the calculation. The average energy is 24.6 keV (using filter 0.8 mm filter) (This data was generated from - X-ray spectrum generator for Monte Carlo Calculations).	84
Figure 3.18	Simulation for verification of the experimental setup.....	86
Figure 3.19	Simulation to measure lead Equivalent and shielding power.....	87
Figure 3.20	Examination room, Control room, and Waiting area denoted as A, B and C.....	90
Figure 3.21	Simulation design of the diagnostic X-ray room viewed from the top (x, y -axis). A) Examination room, B) Control panel room and C) Waiting area.....	91
Figure 3.22	Simulation design of the diagnostic X-ray room viewed from the side (z, x -axis) A) Examination room, B) Control panel room and C) Waiting area.....	92
Figure 3.23	Geometric view from the top (with ictrl=8) of the diagnostic room using the geometrical code before initiating the simulation process.	96

Figure 3.24	Geometric view from the side (with ictrl=8) of the diagnostic room using the geometrical code before initiating the simulation process.	96
Figure 4.1	Cross-sectional image of sample C1-S1 magnified at 400x, 1000x, and 25,000x. a. Open pores, b. Closed pores (bubbles), c. Peak structure..	103
Figure 4.2	Surface microscopic cross-sectional images viewed at 1,000x and 25,000x for sample C1-S1 focusing on the shape of the pores and the detailed structure of the cross-sectional image. a. Open pores, b. Closed pores, c. Peak structure and d. Fused structure.....	104
Figure 4.3	Image of the surface of sample C1-S1 magnified at 400x, 10,000x, and 25,000x. e. Dentation, f. Crystalline.....	105
Figure 4.4	FESEM Surface and cross-sectional images of sample C2-S2 magnified at 400x, 1000x, 10,000x and 25,000x. a. Open pores, b. Closed pores, c. Peak structure, f. Crystalline g. micrograin.	107
Figure 4.5	FESEM surface and cross-sectional images of sample C3-S3 magnified at 400x, 1000x, 10,000x and 25,000x. a. Open pores, b. Closed pores, c. Peak structure e. Dentation, h. unevenly glazed or painted.....	108
Figure 4.6	FESEM surface and cross-sectional images of sample C4-S8 Magnified at 400x, 1,000x, 10,000x and 25,000x. a. Op`en pores, e. Dentation, h. unevenly glazed or painted.	109
Figure 4.7	FESEM cross-sectional images of sample C5-S9 magnified at 400x, 1,000x, 10,000x and 25,000x. a. Open pores, b. Closed pores, e. Dentation, h. unevenly glazed or painted.	110
Figure 4.8	FESEM cross-sectional images of Sample C6-S10 magnified at 400x, 10,000x and 25,000x. a. Open pores, b. Closed pores, e. Dentation, h. unevenly glazed or painted.	111
Figure 4.9	FESEM cross-sectional image of Sample C7-S12 magnified at 400x, 1,000x, 10,000x and 25,000x.	112
Figure 4.10	FESEM cross-sectional image of sample C8-S4 magnified at 400x, 1000x and 25,000x.	113

Figure 4.11	FESEM Cross-sectional images of sample C9-S5 magnified at 400x, 1000x and 25,000x.	114
Figure 4.12	FESEM Cross-sectional images of sample C10-S6 magnified at 400x, 10,000x and 25,000x.	115
Figure 4.13	FESEM Cross-sectional images of sample C11-S7 magnified at 400x, 10,000x and 25,000x.	116
Figure 4.14	FESEM Cross-sectional image of sample S12-S11 magnified at 400x, 10,000x and 25,000x.	117
Figure 4.15	Analysis of area fraction pores for sample ceramic sample tile C1-C6 using Fiji ImageJ.	124
Figure 4.16	Analysis of area fraction pores for sample ceramic sample tile C1-C6 using Fiji ImageJ.	125
Figure 4.17	Linear attenuation coefficient (LAC) for sample C1 to C12 versus.....	140
Figure 4.18	HVL (cm) versus energy ranging from 40 to 150 kV.	142
Figure 4.19	MAC for ceramic tile sample versus energy.	145
Figure 4.20	Mean Free Path against kV energy for Energy ranging from 40 to 150 kV.	147
Figure 4.21	Thickness Required to Attenuate More Than 99% of Radiation for Ceramic Tile Sample C3-C3, C5-S9 and C8-S4 at 40 kV.....	157
Figure 4.22	Thickness Required to Attenuate More Than 99% of Radiation for Ceramic Tile Sample C3-C3, C5-S9 and C8-S4 at 80 kV.....	160
Figure 4.23	Thickness Required to Attenuate More Than 99% of Radiation for Ceramic Tile Sample C3-S3, C5-S9 and C8-S4 at Energy 150 kV	163
Figure 4.24	Shielding Capability Equivalent to 2 mm (0.2 cm) Thickness of Lead.	166
Figure 4.25	Fluence distribution (at energy 150 kV) for sample C5-S9 along x-axis (along direction of the source) at thickness of 20 cm.	168
Figure 4.26	Fluence distribution (at energy 150 kV) for sample S9 ceramic tiles along x-axis (along direction of the source) at thickness of 5 cm.	168

Figure 4.27	Fluence distribution (at energy 80 kV) for sample S9 ceramic tiles along x-axis (along direction of the source) at thickness of 5 cm.....	169
Figure 4.28	Fluence distribution (at energy 40 kV) for sample S9 ceramic tiles along x-axis (along direction of the source) at thickness of 5 cm.....	169
Figure 4.29	Distribution of fluence from the top view using 5 cm thick wall at a spectral energy of 40 kV.....	172
Figure 4.30	Distribution of fluence from the top view using 5 cm thick wall at a spectral energy of 80 kV.....	172
Figure 4.31	Distribution of fluence from the top view using 5 cm thick wall at a spectral energy of 150 kV.....	173
Figure 4.32	Distribution of fluence from the side view using 5 cm thick wall at a spectral energy of 40 kV.....	174
Figure 4.33	Distribution of fluence from the side view using 5 cm thick wall at a spectral energy of 80 kV.....	174
Figure 4.34	Distribution of fluence from the side view using 5 cm thick wall at a spectral energy of 150 kV.....	175

LIST OF SYMBOLS AND ABBREVIATIONS

%	Percentage
°C	Degree in Celsius
μ	Linear attenuation coefficient
μ/ρ	Mass attenuation coefficient
Al	Aluminium
Al ₂ O ₃	Aluminium oxide
AMDI	Advanced Medical and Dental Institute
Ar	argon
BR	Brazil
C	carbon
C++	C Object-Oriented Programming Language
C-C	Carbon-carbon bond
C-O-C	Carbon-oxygen-carbon bond
Ca	calcium
CaF ₂	Calcium fluoride
CAN	Canada
cGy	centiGray
CHN	Carbon, hydrogen, nitrogen
Cl	chlorine
CT	Computed Tomography
Cu	Copper
cm	centimetre
DICOM	Digital Imaging and Communication in Medicine
Dir	Direction

e-type	Energy Type
emin	Minimum energy cut-off
EDX	Energy dispersive X-ray
eV	Electron Volt
EGSnrc	Electron Gamma Shower by National Research Council
FESEM	Field Emission Scanning Electron Microscope
Fe	Iron
FLUKA	Fluktuierende Kaskade
FR	France
FTIR	Fourier Transform Infrared
g	gram
$\text{g}\cdot\text{cm}^{-3}$	gram per centimetre cubic
GATE	Geant4 Application for Tomographic Emission
GEANT	Geometry and Tracking
GLOBOCAN	Global Cancer Observatory: Cancer Today
Gy	Grey
H	hydrogen
HVL	Half-value Layer
ICRU	International Commissioning of Radiation Units and Measurement
ICRP	International Commission on Radiological Protection
ISO	International Organization for Standardization
JIS	Japanese International Standard
JPA	Jabatan Perkhidmatan Awam
K	potassium
KBr	Potassium bromide
keV	Kilo electron Volt
kg	kilogram

kV	kilovolt
kVp	Kilovoltage potential
LAC	Linear Attenuation Coefficient
LEGe	Low Energy Germanium
LiF	Lithium fluoride
MA	Massachusetts
mAs	milliAmpere-second
MAC	Mass attenuation coefficient
mat[n]	Material
M A R A	Majlis Amanah Rakyat
Maxcas	The total number of histories
MC	Monte Carlo
MCNP	Monte Carlo Neutron Positron
MeV	Mega electron Volt
min	minimum
Mg	magnesium
Mn	Manganese
Mo	Molybdenum
MOR	Modulus of rupture
MPa	Mega-Pascal
MV	Megavoltage
MeV	Megaelectron Voltage
N	nitrogen
Na	sodium
NaCl	Sodium chloride
NCRP	National Court Reporters Association
Nb	Niobium

nC	Nano-Coulomb
NIST	National of Institute Standard Technology
O	oxygen
PHITS	Particle and Heavy Ion Transport System
Proj	Projection
QA	Quality Assurance
R	Roentgen
ROI	Region of interest
RPP	rectangular parallelepiped
RM	Ringgit Malaysia
RT	Radiotherapy
R _z	Mean peak-to-valley height
S	sulphur
s-type	source type
Si	silicon
Sn	tin
SO	spherical object
spp.	species
SPECT	single photon emission computed tomography
SSD	source to surface distance
Sv	Sievert
Ti	Titanium
Tofact	Global scaling factor
US	United States
USA	United States of America
UiTM	Universiti Institut Teknologi MARA
USM	Universiti Sains Malaysia

WED	wedge
WT	weighting factor
X	exposure
XCOM	X-ray computed
XRD	X-ray diffraction
XRF	X-ray fluorescence
Z	Atomic number
Z/A	atomic number/mass number of an atom
Z_{eff}	Effective atomic number

PERINCIAN DAN SIFAT PERISAIAN SINARAN PADA BAHAN SERAMIK KOMERSIAL MENGGUNAKAN ALUR FOTON KILOVOLTAN

ABSTRAK

Kajian ini adalah bertujuan untuk menilai kesesuaian seramik sebagai bahan perisai sinaran bagi sinar-X kilovoltan, khususnya dalam konteks bilik pengimejan diagnostik. Struktur dinding konvensional untuk ruangan seperti bilik biasanya terdiri daripada kombinasi konkrit, bata, plaster barium, dan plumbum. Namun demikian, plumbum berpotensi membawa risiko kesihatan sekiranya berlaku pendedahan berpanjangan. Sebagai alternatif, seramik dikenalpasti sebagai bahan perisai sinaran yang lebih mesra alam, selamat dan mampan. Kajian ini memfokuskan kepada pemeriksaan terhadap 12 sampel seramik yang dilabel sebagai C1-S1 hingga C12-S11. Setiap sampel dianalisis menggunakan mikroskop elektron imbasan pancaran medan (FESEM), spektroskopi tenaga sinar-X (EDX), dan spektroskopi sinar-X pancaran sinar (XRF) untuk menilai perincian struktur, morfologi, kandungan unsur, dan kadar peratusan unsur-unsur seramik tersebut. Ujian sinaran dalam julat tenaga diagnostik turut dijalankan bagi menentukan sifat perisai setiap sampel seramik. Tiga sampel terbaik iaitu C3-S3, C5-S9, dan C8-S4 telah dipilih untuk verifikasi lanjut dan simulasi. Setiap sampel seramik menunjukkan perbezaan ketara dari segi struktur permukaan, dan morfologi. Sampel C5-S9, yang mempunyai bilangan pori tertutup dan terbuka paling sedikit serta kandungan logam yang tinggi, didapati memiliki ketumpatan paling besar, menjadikannya lebih sesuai sebagai bahan perisai sinaran. Dari segi pekali pelembapan linear (LAC), sampel C5-S9 mencatat nilai tertinggi pada 4.58 cm^{-1} pada 40 kV dan 1.39 cm^{-1} pada 150 kV. Nilai pekali pelembapan jisim (MAC), lapisan nilai separuh (HVL), dan purata laluan bebas (MFP) bagi sampel ini juga menunjukkan prestasi perisai sinaran yang lebih baik berbanding sampel lain,

dengan nilai MAC dan HVL masing-masing pada 40 kV adalah 1.87 cm²/g dan 0.151 cm. Perbandingan nilai LAC seramik C5-S9 melalui simulasi menggunakan sistem kod pengangkutan zarah dan ion berat (PHITS) dengan hasil eksperimen menunjukkan perbezaan kecil dalam julat 0.4% hingga 4.8%. Keputusan ini menunjukkan bahawa ketebalan minimum 1.4 cm bagi sampel C5-S9 diperlukan untuk mengurangkan kadar sinaran sehingga 99.91% pada 40 kV, manakala ketebalan 12 cm diperlukan pada 150 kV. Berdasarkan analisis yang dijalankan, seramik berpotensi tinggi untuk menjadi bahan perisai sinaran yang efektif bagi bilik pengimejan sinar-X diagnostik.

CHARACTERISATION AND RADIATION SHIELDING PROPERTIES OF COMMERCIAL CERAMIC MATERIALS USING KILOVOLTAGE PHOTON BEAM

ABSTRACT

The study evaluate the suitability of ceramics for radiation shielding in terms of their characteristic and shielding properties. The usual wall construction for diagnostic imaging rooms consists of a certain thickness of concrete, bricks, barium plaster and lead. However, lead is harmful to health, in the long term. Alternatively, ceramics are a more sustainable source of radiation shielding compared to lead. This study is focus on examining twelve (12) different types of ceramic samples labelled as C1-S1 to C12-S11. Each ceramic sample were examined using field emission scanning electron microscopy (FESEM), energy dispersive X-ray (EDX) and X-ray Fluorescence (XRF) analysis to assess the characteristics of the ceramic structures, including topography, morphology, elemental content, and percentage. An experimental setup to determined the radiation shielding properties was performed for all the ceramic samples. Among all the ceramic sample, C3-S3, C5-S9 and C8-S4 were selected for varification and simulation using Particle and Heavy Ion Transport Code System (PHITS) software. Each sample shows variation in surface structures with C5-S9 having the lowest number of open and closed pores, and fused structures. C5-S9 also has high iron content and density, which would be suitable for shielding. Sample C5-S9 exhibited the highest LAC value of 4.58 cm^{-1} at 40 kV, and 1.39 cm^{-1} at 150 kV. In terms of mass attenuation coefficient (MAC), half-value layer HVL, and MFP sample C5-S9 also showed greater shielding capabilities compared to the other samples, with the values MAC and HVL at 40 kV being 1.87 and 0.151 cm respectively. The LAC value of the ceramic C5-S9 was then measured using MC

PHITS and compared to the experimental setup, with smaller differences found ranging from 0.4 to 4.8%. The result shows that C5-S9 requires the least thickness of 1.4 cm to reduce radiation to 99.91% at 40 kV and 12 cm at 150 kV. The fluence distribution was developed for 5 cm thick wall at energy range 40 to 150 kV. The intensity is highest in the primary beam area and decreases with increasing distance from the source. Conclusion With careful consideration, ceramics could be a good shielding material for diagnostic X-ray rooms.

CHAPTER 1

INTRODUCTION

1.1 Background

Radiation protection and safety is an issue that is in the interest of protecting patients, radiation safety personnel, and the public (Hamad et al., 2020; Olukotun et al., 2020; Ripin et al., 2019; Suhaiman et al., 2018). High radiation dose and exposure can lead to radiation sickness and harm individuals. Therefore, gaining knowledge on radiation safety could reduce radiation risk while maintaining the effectiveness of the procedure (Mitchell and Furey, 2011). Guidelines for Radiation Protection has been published to protect the rights of patients, the public, and radiation personnel.

In recent decades, demand for medical imaging examinations, including radiological examinations and computed tomography scans, has increased sevenfold, leading to an increase in service workload (Kwee & Kwee, 2021; Berrington De Gonzá Lez et al., 2009;). Clinical practice research in the United Kingdom has reported that the number of diagnostic tests has increased threefold compared to 15 years ago, with an average of 5 tests per year per patient (Torjesen, 2018).

The increasing number of examinations has brought concerns about radiation exposure to workers and patients (Alajerami et al., 2020; Jawad et al., 2019). Reference levels have been introduced to reduce radiation dose. Radiation protection programme was adopted to eliminate radiation and reduce the risk which applies the principles of using optimal time, increasing distance, and applying adequate shielding between the radiation source and radiation workers or the patient. However, the main approach of

radiation protection focuses more on shielding used for the X-ray room (Jawad et al., 2019).

The purpose of safe structural shielding design in medical imaging facilities is to ensure the safety of radiation protection personnel and the public from hazard of radiation. Physicists and radiation protection personnel must be constantly aware of the primary and scattered radiation that may occur (Mitchell and Furey, 2011) especially in low energy diagnostic settings. The National Council on Radiation Protection and Measurement (NCRP Report No. 147, 2004) suggested that medical imaging facilities to have a designated controlled area (an area with limited access for personnel under the supervision of radiation protection officer) and another uncontrolled area surrounding the controlled area with optimal shielding.

At the same time, the International Commission on Radiological Protection (ICRP) have also constantly reminded medical imaging provider to comply to “current standards of radiation protection to avoid unnecessary radiation by keeping the doses below relevant threshold and ensure sufficient precaution are taken to reduce the occurrence of stochastic effects”. The effectiveness of radiation shielding is highly dependent on the photoelectric attenuation coefficients of the materials used, the thickness of the material used, and the energy spectrum of the radiation (McCaffrey et al., 2007). At the same time, constant maintenance, and monitoring of the integrity of the shielding in the facility are part of the measure to eradicate scattered radiation that contribute to the increase in dose to workers and the public.

Conventional shielding structure for the diagnostic radiology room for the wall and ceiling consists of a combination of concrete, barium plaster, bricks and lead slab, which were used as a means of protection against ionising gamma and X-ray radiation.

Lead was chosen because it has a high atomic number (Z) (82) and density (11.5 g/cm^3). However, lead has certain disadvantages, for example, it is toxic and carcinogenic. In addition, lead is also heavy, has low mechanical strength, and is inflexible (Al-Hadeethi et al., 2020; Lermen et al., 2020). This has led researchers to investigate different types of shielding materials such as ceramics, concrete, barite, marble, and other materials. Ceramics were chosen as the motive for this study because they have been shown to have higher strength, higher modulus, and lower wear resistance compared to other materials (Salehi et al., 2015).

In principle, some properties of ceramics have a structure that resembles concrete including being inorganic, non-conductive, non-metallic and non-corrosive properties. The material composition consists of quartz, kaolin, and mullite compounds. Ceramics are also manufactured in various types, shapes, and sizes (Griggs et al., 2002) which are suitable to be used for variety purposes in building and construction, including ceramic pipes, ceramic floor tiles, and roof tiles. The recent modification and designs of ceramics has increased the efficiency of manufacturing ceramics to achieve strong structural integrity and high quality to supply the local and global market. Nanotechnology makes it possible to better understand the atomic and molecular structure of materials, which makes ceramics indispensable for development and improvement in the future.

The use of ceramics has expanded to potential applications in the medical field such as medical devices, medical pumps, drug delivery devices, scaffolds for tissue engineering, and blood shear valve (Allameh and Sandhage, 1997; Xiao-Dong Zhang et al., 1997) and the fabrication of cast ceramic prostheses due to their high radiopacity, strong durability, and high tensile strength. There are also demands of using barium

aluminosilicate phosphate glass-ceramics for patient immobilization due to its radiopacity properties and ability to contain radioactive material (Caurant et al., 2007). The need of ceramic has also extended in imaging devices such as dental and mammography equipment, barium and glass-ceramic matrix mixtures have been used as common composites for radiopaque filters. Ceramics have also been used as base materials due to the stability of the material. Apart from this, barium ceramics could be a potentially plausible material for the design of an X-ray room.

In recent years, a variety of novel composite materials have been investigated to find a potential shielding material that comply the radiation safety criteria (Asal et al., 2021). Studies using heavy metal fluoride-based tellurite-rich glasses have been developed for gamma radiation shielding (Sayed et al., 2018). In another study, a bismuth compound with natural rubber was proposed as the main material for shielding against X-rays and gamma rays. (Intom et al., 2020). Other types of radiation shielding such as barium bismuth borosilicate glasses have been investigated (Bootjomchai et al., 2012). The outcome for this study suggests that high-density materials, such as barium bismuth borosilicate, are suitable as radiation shielding materials, unlike conventional radiation shielding concretes (Cheewasukhanont et al., 2020; Ripin et al., 2019). Polydimethylsiloxane/bismuth (III) oxide composite material has shown the same result (Dubey et al., 2014). This has made ceramic compounds a suitable applicant for radiation shielding because they contain a reasonable number of metals and oxides, as well as high density.

Factors such as weathering and aging can abuse the structure and cause it to become brittle and crack, making it difficult to find a mere equal shielding material with a robust and dynamic structure. The Atomic Energy Licensing Board (AELB)

recommended enough barium plaster to oppose against radiation. The Malaysian Occupational Radiation Protection Guidelines suggest that the attenuation capability of new shielding materials must be tested before they are approved for shielding. As mentioned in the Malaysian Guidelines for Occupation Radiation Protection, shielding properties equivalent to lead could be used as a guideline to test the effectiveness of the shielding material. On the contrary, ceramics have been reported to have strong structural integrity, low thermal expansion that can withstand high temperatures (above 1200 °C), high oxidation resistance, are environmentally friendly, and have a low dielectric constant (Ripin et al., 2019). The objective of this study is to evaluate the radiation properties of commercial ceramic tiles by assessing the microsurface structure, measuring the attenuation properties of the ceramic, and providing MC simulation model. To our knowledge, there are few studies and findings on ceramic tiles as shielding materials. Figure 1.1 illustrates the workflow of this study.

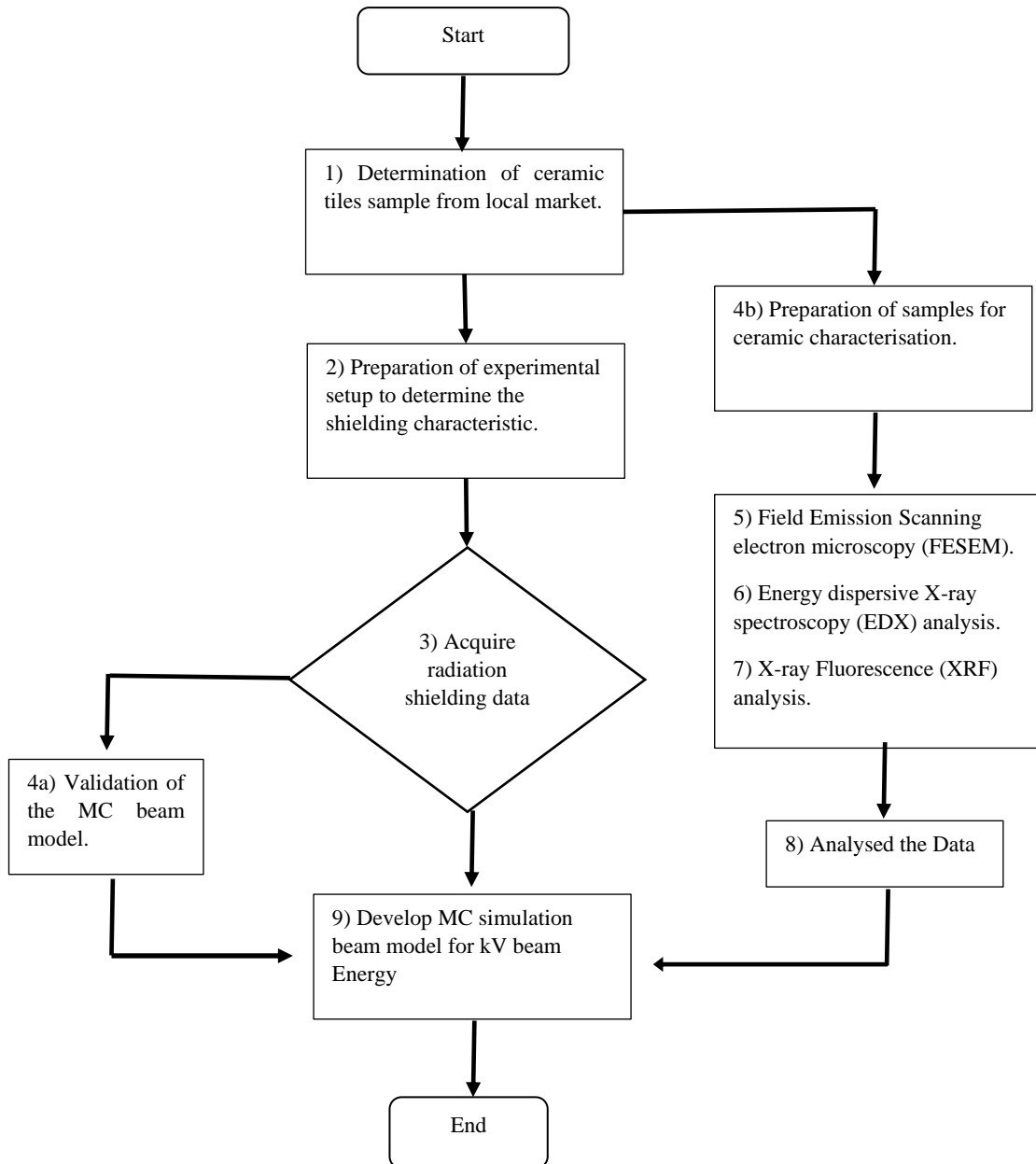


Figure 1.1 The workflow towards the evaluation of ceramic tiles.

1.2 Problem statement

In designing an X-ray/gamma-ray room, various parameters should be considered, including the safety of radiation personnel, radiation energy, design for the room for radiation interaction, thickness of the shielding material, and cost of the shielding material.

Traditionally, lead has been used as a radiation shielding material to provide a safe environment for radiation personnel. However, lead material is highly toxic, limited, and expensive. Ideally, radiation shielding should be made of a material that would be able to reduce the radiation to acceptable levels; therefore, high-density materials or material equivalent to lead may be considered as a substitute for this material. In addition, future shielding materials should be cheap, strong, durable, robust, and readily available in the market. The study on shielding is now being extended to other types of materials that are suitable to replace or reduce the use of lead.

Studies have suggested the use of high-density materials for shielding in diagnostic and therapeutic radiation rooms, such as cement, barium, lead, or other suitable high-density materials. A considerable number of materials have been developed and studied to find the best material for the radiation energy used (Kavaz, 2019; Obaid et al., 2018; Yao et al., 2016; Kharita et al., 2008). Therefore, ceramics should be investigated as a potential radiation shield since it is likely to have the same density as concrete.

Practical parameters use to evaluate the safety of radiation shielding in a room or building include mass attenuation coefficients, energy absorption coefficients, and half-value layer (Singh and Badiger, 2013). Other factors to consider are the safety of the radiation worker, the radiation energy or radiation instrument used in the examination, the design of the X-ray room, the thickness of the shielding bunker, and the cost of the shielding material when designing an X-ray/gamma-ray room facility.

Finding material that meets the listed criteria used to be a challenging and difficult task. However, extensive research in this subject have led to the development of new formulations and adaptations of radiation material. Certain types of ceramics are

suitable for specific characteristics based on the application, including ceramic tiles (Al-Ghamdi et al., 2022) that has brought the interest of this current study to evaluate the shielding properties of available ceramic tiles in the market. Local ceramic tiles were chosen as the subject due to their availability and cost effectiveness compared to other materials, such as lead or barium plaster. In addition, ceramic tiles have several particular shielding criteria such as low density ($2-6 \text{ g/cm}^3$), easy to maintain, non-toxicity to humans and the environment, cost effective and easily available in the market compared to metal oxides or lead.

1.3 Objective of research

The objectives of this study are to evaluate, validate, and calculate ceramic tiles, in an attempt to provide expanded and extended data in terms of the shielding capabilities and material properties of ceramic. This study focuses on following objectives:

- i. To characterise ceramic material properties using Field Emission Scanning Electron Microscope (FESEM), Energy Dispersive X-Ray (EDX), and X-ray Fluorescence (XRF) analysis.
- ii. To evaluate shielding characteristic data for kV photon beam.
- iii. To establish a validated MC beam model from kV beam energy.

1.4 Significance of study

The research and data presented in this study are useful for expanding the current understanding of ceramic tiles available on the market as shielding materials. Broad data sets derived from ceramic characteristics, shielding properties, and the validated

Monte Carlo beam model for kV beam energy will provide further information on the development of shielding barriers specifically for diagnostic rooms or energy.

Detailed element information for different types of ceramics provided during the characteristic analysis will be useful for comparison with other types of shielding materials, such as barium plaster or lead. Element data is also important for determining the attenuation properties of ceramic tiles and comparing them with lead or other materials used for radiation shielding. The surface and cross-sectional images are useful because they provide data on the image topography and geometry of the ceramic at high magnification. These data provide information about the surface structure of the ceramic tiles.

Data on the shielding characteristic of ceramic tiles provides information on the attenuation properties and half-value layer of the material under study. This data is useful both individually and in aggregate, as they provide knowledge and understanding of the shielding capabilities of ceramic tiles on the market.

The validation of the simulation is useful because it provides validated data representing the ceramic elements and experimental setup of this study. The validated simulation process using Monte Carlo is functional to help researchers measure exposure/dose using the data available in this study.

1.5 Outline of thesis

This document contains 6 chapters. Chapter one emphasized the rationale of this study include the introduction of the study, which consists of the background of this study, problem statement, objectives of research, and significance of study. Second chapter is the literature review, which covers theory of interaction, attenuation coefficient,

mass attenuation coefficient and half-value layer, radiation concept and units, radiology diagnostic room design and shielding.

The third chapter is to fulfil the first objective of “characterise ceramic material using Field Emission Scanning Electron Microscope (FESEM), Energy Dispersive X-Ray (EDX), and (X-ray Fluorescence XRF) analysis”. This chapter provides structure geometry, and topography data of the ceramic tiles chosen for this study. The results from the elemental data were also crucial in the contribution of data for scientific work related to the ceramic study.

Chapter 4 investigates the shielding property of ceramic tiles. This includes the exposure data which is then converted to linear attenuation coefficients (LAC), half-value layer (HVL), mass attenuation coefficients (MAC), mean free path (MFP), and other related shielding characteristic data for all the ceramic samples.

Chapter 5 is dedicated in designing a Monte Carlo (MC) Modelling, simulation and validation of the ceramic material using the Particle and Heavy Ion Transport Code System (PHITS) MC simulation software. Using the data elemental and geometrical room Chapter 6 concludes this study and recommends improvement for future of this ceramic study.

1.6 Scope of Study

The scope of this study entails the evaluation of ceramic as shielding in photon beam kilovoltage (kV). Thus, it requires the researcher of this study to acquire the relevant data related to the ceramic as shielding in diagnostic setup that includes the characterisation of ceramic, shielding characteristic data and provide Monte Carlo (MC) validated modelling.

The first phase of this study includes exploring the surface and cross-sectional structure of the ceramic tiles in study. This would require characterising the ceramic tiles in study. The rationale characterising the ceramic tiles samples are simply to understand the microstructural and elemental composition of ceramics that are crucial for assessing their suitability as radiation shielding materials. FESEM were chosen as the equipment that provides high-resolution microimages that has structural integrity of the ceramic surface and cross section. EDX and XRF offer elemental analysis, aiding in identifying elements and component of the ceramic tiles affecting shielding properties.

The quantification of shielding effectiveness involves measuring parameters such as attenuation coefficients and transmission factors related to kV photon beam. This were done to establish empirical data on how effectively the ceramics reduce radiation exposure at energy beam typical to medical diagnostic setting. Thus, this study has to employs medical imaging kV photon beam setup to evaluate the shielding of the ceramic in study.

PHITS MC simulations are essential for predicting complex radiation interactions accurately. Validating the model against experimental data ensures reliability in predicting shielding performance under various conditions. This method of PHITS simulation bridges theoretical simulations with practical experimental results, enhancing the predictive capability and understanding of ceramic materials' suitability for radiation shielding applications.

CHAPTER 2

THEORY & LITERATURE REVIEW

2.1 X-ray Interactions

The smallest unit of matter, known as the 'atom', consists of electrons orbiting around a central nucleus. The nucleus itself contains proton (as positive charge) and neutrons. The proton stands for the atomic number, Z and there are as many electrons orbiting the nucleus. The nearest orbit to the nucleus (which has the strongest bond) is in order of K, followed by L, M, N. Excitation, and ionisation of the electron in an atom are the two basic process for understanding most radiation interactions, which are relevant to radiation shielding, biological effects, radiation instrument and many other processes (Carolyn A. MacDonald, 2017; Michael G. Stabin, 2008)

These electrons are stable as long as they are not excited or ejected from the orbit. The process of ejecting the electron from the orbit is known as ionisation. The ionisation and excitation process is related to the interaction of X-ray photons with matter. Excitation refers to the excited state of the electron from the lower band of the orbit to the higher band. Differently from excitation, Ionisation of electron is the situation in which the electron is completely removed from the orbit. The state where the electron is ejected from an atom, which is called an ionised state. The vacancy left in a low orbital is filled by the capture of a free electron or by the de-excitation of an electron from the outer orbit to the inner orbit (rearrangement of the atomic electron). The incident radiation that interacts must have sufficient kinetic energy (between 4 and 25 eV) to cause ionisation in the orbit (Carolyn A. MacDonald, 2017).

The interaction of X-rays can be summarized into three possible interactions of an X-ray or gamma-ray photon during and after bombardment upon a material. The first interaction happens with the photon being absorbed (all the energy is transferred to the target). The second is that it is scattered or passes through the material without interaction. The whole process of absorption and scattering is called the attenuation process. These interactions that are related to radiology are usually divided into coherent, Compton and photoelectric interactions. In diagnostic radiology, the Compton effect and the photoelectric effect are particularly related and important (Carolyn A. MacDonald, 2017).

Coherent scattering (also called the elastic scattering) is a type of photon interaction that occurs at lower photon energy which interact with an atom. In this case, the photon does not have enough energy to release an electron, so the energy loss is negligible. The photons are usually deflected or scattered at an angle nearly equal to the original path. Coherent scattering is less important because little/no energy is released to the medium and it provides less information about the attenuating material. It also does not contribute to the diagnostic image as the photon is diverted or scattered. This interaction usually occurs when a photon has energy less than 10 keV (Walter Huda and Richard M. Slone, 2003).

Figure 2.1 shows a diagram of the coherent scattering. Coherent scattering occurs when the initial low energy photon interacts with the atom, deflecting the photon in a direction close to the initial trajectory, with the almost same wavelength and energy. It is also known as Rayleigh or classical elastic scattering (Bushberg et al., 2020)

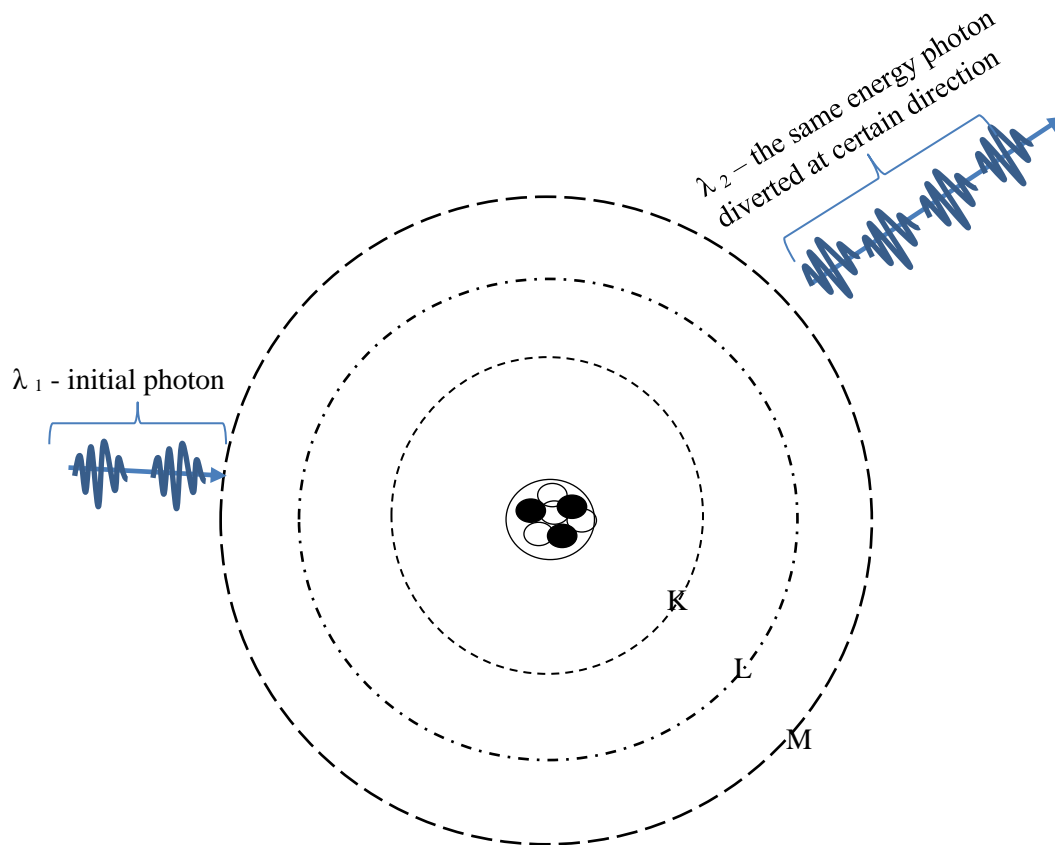


Figure 2.1 A diagram of the phenomenon of coherent scattering. Model were adapted from The Essential Physics of Medical Imaging (4th ed.) by Bushberg, Seibert, Leidholdt, and Boone, coherent scattering (Rayleigh scattering) Chapter 3, Page 39

Photoelectric interaction is a type of interaction where the initial photon traversing is transferred to the electron, which is then ejected out from the atom. For this to happen, the energy of the incident photon must be equal to or greater than the binding energy causing the energy to completely absorb. The photoelectric interaction decreases as the energy of the photon increases. However, the photoelectric interaction increases with a higher atomic number up to the factor of Z^3 . The photoelectric interaction takes place in the inner valence orbital of the shell and the electron ejected from the atom called the photoelectron. The absorbed photon contributes significantly to the value of

the absorption coefficient in this interaction. In this type of interaction, there is no scattering of the photon (Huda, W., & Slone, R. M. 2016).

Compton scattering or inelastic scattering occurs when a photon collides with an electron, resulting in an ionisation of the electron and partial loss of X-ray energy due to the interaction. The energy produced by the Compton effect depends on and is equal to the energy lost during the bombardment. This results in the electron being ejected at a random angle of at most 90° from its original trajectory. The trajectory angle of the ejected electron is an angle with respect to the direction of the initial photon. The probability that Compton scattering to occur is inversely proportional to the energy of the photon but is independent of the atomic number. In diagnostic imaging, Compton scattering reduces the quality and resolution of the image and adds an unnecessary dose to the patient. However, the energy deposited during the process contributes to the value of the absorption coefficient, which is important for determining shielding characteristic (Huda et al., 2000).

As figure 2.2 indicate, the incident X-ray beam (labelled A) strikes the electron in an atom and excites it (labelled as B). When the vacated orbit is filled with electron from the upper orbit, an X-ray photon is produced at a different angle. The scattered X-rays have the same energy as the original incident X-rays, but in a different direction (or deflected) (Huda et al., 2000).

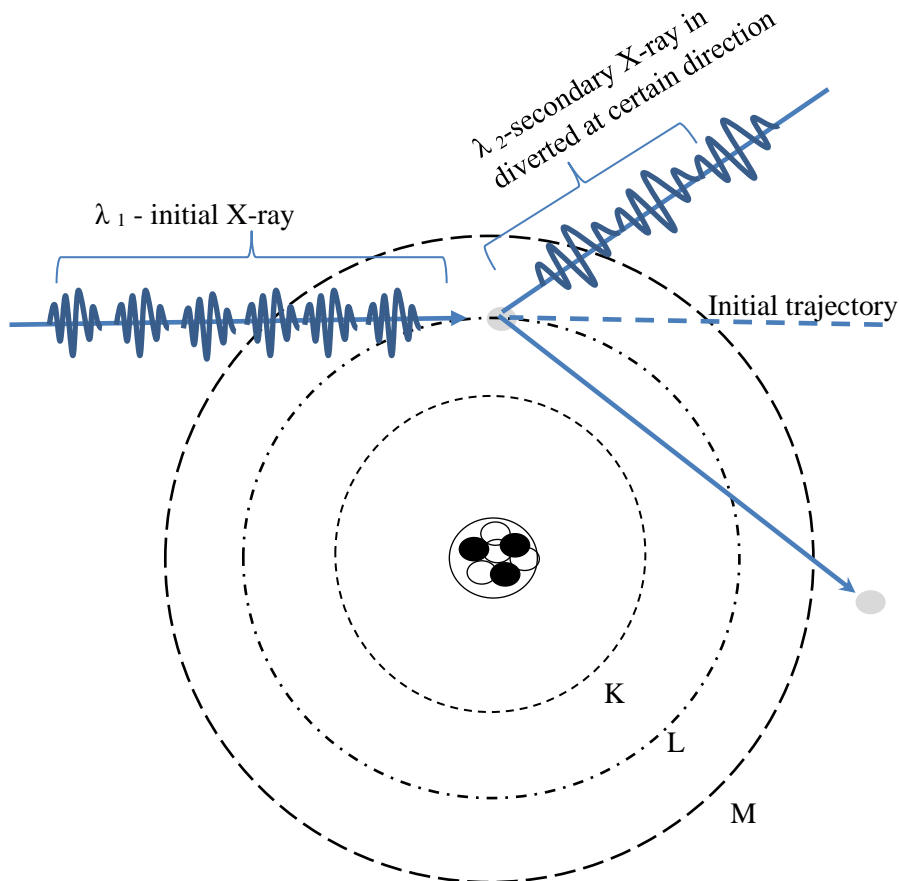


Figure 2.2 A Model Diagram of Compton scattering adapted from The Essential Physics of Medical Imaging (4th ed.) by Bushberg, Seibert, Leidholdt, and Boone chapter 3, Page 40.

X-ray radiation has a wavelength of 10^{-8} to 10^{-10} meters, which provides useful information about the target material when it interacts with matter (atoms). When an X-ray beam passes through a medium, it is attenuated, and the degree of attenuation depends on the material and the energy.

Useful radiation for diagnostic and therapeutic purposes has an energy range from 3 keV to 7.0 MeV (Bushberg et al., 2020). Ionising and non-ionising radiation are distinguished by energy and wavelength. Lower energies are classified as non-ionising radiation because their energy is low, and they cannot penetrate or ionise. Higher energies of radiation are called ionising radiation, which is divided into directly ionising radiation (electrons, protons, alpha particles) and indirectly ionising radiation

(photons and neutrons) (Podgoršak, 2016). When the radiation interacts with the target material, the total energy is always conserved. However, the number of particles is not conserved, as they can be absorbed, deflected, or transmitted during the procedure (Bushberg et al., 2020).

2.2 Radiation Shielding Properties

A mathematical expression to calculate the ability of material to attenuate through a material is measured using transmission factor. Transmission is the amount (intensity) radiation passing through a given thickness of material (Seibert, 2019). Given the photon is monoenergetic and directed to a narrow geometry, then the intensity (I) of photon penetrating of a slab of a matter thickness is as in Equation 2.1.

$$I = I_0 e^{-\mu x} \quad \text{Eq. 2.1}$$

where μ is the attenuation coefficient of the medium for the photons and I_0 is the number of photons in the beam before any slab absorber material with certain amount of thickness is placed into position in between the source and detector. In general, attenuation coefficient varies with the radiation energy of the photon and the atomic number of materials, providing useful information about the material of study (Seibert, 2019). The linear attenuation coefficient of the material was represented as Equation 2.2.

$$\mu = \frac{1}{x} \ln \left(\frac{I_0}{I_t} \right) \quad (\text{Eq. 2.2})$$

Secondary or scattered radiation that deviate from the original pathway should be excluded from the equation as it does not represent the actual initial intensity of photon beam. Photons lose energy from the interactions and produces secondary or scattered radiation (due to the collision) and deviated from the trajectory pathway. Scattered radiation that manages to penetrate the absorber could be excluded by applying some distance from the absorber to the detector.

In a broad-beam geometry, a narrow-beam attenuation setup is attained by collimating the X-ray window to a maximum angle of 3° or using a 1:10 ratio of the field view to the source-to-detector distance. As consequence Equation 2.2 remains valid under these conditions even for real beam of uncharged primary radiation (Bushberg et al., 2020).

The logarithm of initial photons intensity exhibits a linear inverse relationship with the thickness of the material studied. Consequently, a linear graph relationship can be obtained for a given material thickness and corresponding intensity. In a broad-beam geometry setup, scattered radiation causes the intensity to decrease less rapidly, which is significant factor when designing shielding walls for diagnostic X-ray room energy. The beam energy emitted from a general X-ray tube is poly energetic, meaning it cannot be represented by a single attenuation coefficient. However, it can be described by weighing the average of exponential equations for each of the different energies in the beam. This representation is known as effective linear attenuation coefficient, which also depends on effective atomic number (Z_{eff}) of the material. To produce a monoenergetic photon, diagnostic units are incorporated with added filtration of 1-3 mm aluminium (Bushberg et al., 2020). To compensate poly energetic photon beam in a diagnostic radiology setting, an effective attenuation coefficient can be used as can be seen in Equation 2.3.

$$\mu_{\text{eff}} = \frac{\ln 2}{HVL} \quad (\text{Eq. 2.3})$$

The effective energy of an X-ray beam is defined as the energy of monoenergetic photons that have an attenuation coefficient in a specific medium equivalent to the effective attenuation coefficient of the X-ray beam in that same medium. However, if the experimental setup is controlled to reduce scattered and secondary radiation, the broad-beam geometry can approximate narrow-beam attenuation, causing the effective linear attenuation coefficient to approach the value of the narrow-beam linear attenuation coefficient.

Another concept used to estimate the shielding capability of a material is the half-value layer (HVL). The HVL is a measure of the material's ability to reduce the intensity of radiation by half. It serves as an indicator of both the quality and intensity of the beam. The HVL depends on several factors, including the type of material, the type of radiation, the energy of the radiation, and the thickness of the material. In the case of a heterogeneous beam, the HVL can be defined using the same effective attenuation coefficient (Bushberg et al., 2020), as described by Equation 2.4.

$$HVL = \frac{\ln 2}{\mu} \quad (\text{Eq. 2.4})$$

Different types of attenuating materials with varying thicknesses are used in the same experimental setup to ensure the accurate determination of the half-value layer (HVL). Radiation dose rates are measured with and without the attenuator in place. To minimize scattered radiation from the attenuator, the attenuating material should be

positioned at least 50 cm from the dosimeter. A broad-beam geometrical setup is typically employed to determine the shielding requirements for primary and secondary barriers surrounding the X-ray machine (Podgorsak, E. B., 2016).

For materials composed of multiple elements, such as ceramics, the bulk density of the material must be considered. The mass attenuation coefficient formula accounts for the material's density. The mass attenuation coefficient is defined as the measurement of the absorption coefficient, which reflects the average number of photons before and after interaction, while also considering the percentage mass of each element and its atomic number (Podgorsak, E. B., 2016). Equation 2.3 for the mass attenuation coefficient is derived from Equation 2.5.

$$\mu_m = \frac{\mu}{\rho} = \sum_i \omega_i (\mu/\rho)_i \quad (\text{Eq. 2.5})$$

where, i^{th} is the element in the material and ω , is the weight of the fraction at i^{th} . The mean free path (MFP) is another parameter used to distinguish the shielding characteristics of the ceramic material. MFP is the estimate of the average distance of a photon passing through any material as a function of the number of collisions. It is inversely related to LAC as shown in Equation 2.6.

$$\text{MFP} = \frac{1}{\mu} \quad (\text{Eq. 2.6})$$

The values of LAC and MAC can also provide data on the electron charge density of the any material, as explained by Langeveld, 2017 by applying Equation 2.7.

$$\sigma = \frac{Z N_A e}{A} \rho \quad (\text{Eq. 2.7})$$

where, Z is the sum of atomic number, A is the material atomic weight, N_A is Avogadro's number, and e is the electron charge. The measured MAC value can also derive the total atomic cross-section (σ_t) by applying Equation 2.8.

$$\sigma_t = \frac{\mu_m \sum n_i \times A_i}{N_A} \quad (\text{Eq. 2.8})$$

Where n_i is the number of atoms of the i^{th} individual's element, and A_i is the atomic weight of the element. The total electronic cross-section is derived from Equation 2.8.

$$\sigma_e = \frac{1}{N_A} \times \sum \left(\frac{f_i \times N_i}{Z_i} \right) \quad (\text{Eq. 2.9})$$

Here, f_i is the fraction abundance of the element i^{th} .

2.3 Radiation Concept and Units

Understanding the fundamental principle and units of radiation is important in ensuring safe application of radiation practices, particularly concerning patient and operator well-being (Mitchell and Furey, 2011). X-rays is a form of radiation that are produced by the transition of electrons within the atomic orbitals, resulting in the emission of discrete photon energy. Consequently, the occurrence of X-ray interacting with a material allows the measurement of radiation within a particular region. The measurement of X-rays provides important information such as the intensity and characteristics of the radiation.

Although the total number of photons at a given point on the target usually provides little meaningful information about the dose to the patient, its use in the context of shielding properties, attenuation, and transmission of radiation is nevertheless beneficial. Total number of photons or the intensity of the photons are used to derive LAC, MAC, and HVL for the data regarding shielding characteristic.

Fluence or photon concentration, is defined as the number of photons traversing through an area of 1 cm^2 during a single irradiation. The total number of photons in any uniformly distributed X-ray exposure is derived from multiplying the concentration of fluence by the exposed area, which is inversely related to the total number of photons imparted to the target.

The amount of ionisation produced in a mass of 1 cm^3 air is the measure of Exposure (X) in unit 1 Roentgen or 2.58×10^{-4} Coulombs/Kilogram of air. X is directly related to the measure of radiation concentration but does not provide information about tissue or organ damage because it does not take sensitivity of the tissue into consideration. The air Kerma (K) is referred to as the kinetic energy imparted from photon per unit mass of air. The relationship between exposure and photon concentration or fluence for a specific photon energy is straightforward because both the number of photons that interact and the number of Ionisations produced by each interaction is dependent on the photon energy. Absorbed dose is measured in unit Gray (Gy), which is defined as equivalent to the absorption of 1 J of radiation energy per kg of tissue. The relationship between these units is simplified in equation 2.9.

$$1 \text{ Gy} = \text{J/kg} = 100 \text{ rad} \quad (\text{Eq. 2.9})$$

In a homogeneous (example muscle) tissue at specific energy spectrum, the absorbed dose is proportional to the exposure delivered to the tissue. However, absorbed dose is not proportional to exposure in an inhomogeneous structure such as the bone. Equivalent doses take into consideration the sensitivity of organ and type of radiation. This equation utilises the weighting factor (WT), that reflects the value of biological damage with respect to the type of radiation. The unit used for equivalent dose is Sievert (Sv).

2.4 Radiology Diagnostic Room Design and Shielding

A recent study by Hamad et al., 2020 has provided evidence that radiation attenuation in diagnostic setting, is optimal at a potential energy of 70 kVp. However, it is important to note that comprehensive data on ionising radiation within the range of 10 keV to 10 MeV has been well-documented in the existing literature and holds relevant across diverse fields dealing with radiation (Hubbell, 1977; Michael G. Stabin, 2008; P.J. Dimbylow and T.M. Francis, 1984).

Diagnostic X-ray devices, commonly used in radiology, are designed to produce radiation with a heterogeneous energy profile in the 40-150 kilovoltage peak (kVp) range over a short duration, typically measured in milliseconds. The specific energy parameters required depend on the radiographic technique and the region being examined, such as the skull, chest, extremities, or spine. Effective photon energy refers to the energy at which the highest intensity is achieved for a selected X-ray energy, whereas kVp represents the maximum energy that can be attained within the chosen energy spectrum. The X-ray tube head, integrated into the radiographic device, is equipped with a housing and radiolucent window, allowing precise directional targeting of the radiation to a specific region, angle, and distance from the patient.

Operators can rotate the X-ray tube to align with the clinical region of interest, optimizing diagnostic results (Zarb, 2024).

Although X-rays are invaluable in medical diagnostics, they pose risks to human cells, particularly to radiation workers if exposure exceeds safety limits. The primary source of exposure for staff arises from handling patients during radiological examinations and operating the equipment. One strategy to reduce radiation exposure is to optimize examination time to suit the patient. However, this approach must carefully balance the need for sufficient diagnostic information with minimizing the examination duration (Zarb, 2024).

An additional method to reduce radiation exposure is through effective radiation protection measures, including the use of high-quality shielding materials to prevent adverse effects (International Atomic Energy Agency, 2018). Enclosing the radiation source in a shielded room is critical to ensuring a safe working environment for radiation workers (Abdul Aziz et al., 2020), which is essential for maintaining the safety of operator during X-ray examination.

Before designing a diagnostic X-ray room, contractors and suppliers must consider the type of shielding material, the room size, and the energy of the radiation source. These factors must comply with regulatory standards, as it is impractical to monitor every examination conducted in the work environment. Therefore, a comprehensive strategy is necessary, including the provision of appropriate shielding materials and determining the optimum room size to ensure radiation safety. Meanwhile, As Low As Reasonably Achievable (ALARA) principles were entirely an alternative precautionary approach aimed at mitigating the exposure to the worker and public.